PB82-153784

Use of Water Raman Emission to Correct Airborne Laser Fluorosensor Data for Effects of Water Optical Attenuation

(U.S.) Environmental Monitoring Systems Lab.
Las Vegas, NV

20 Mar 81

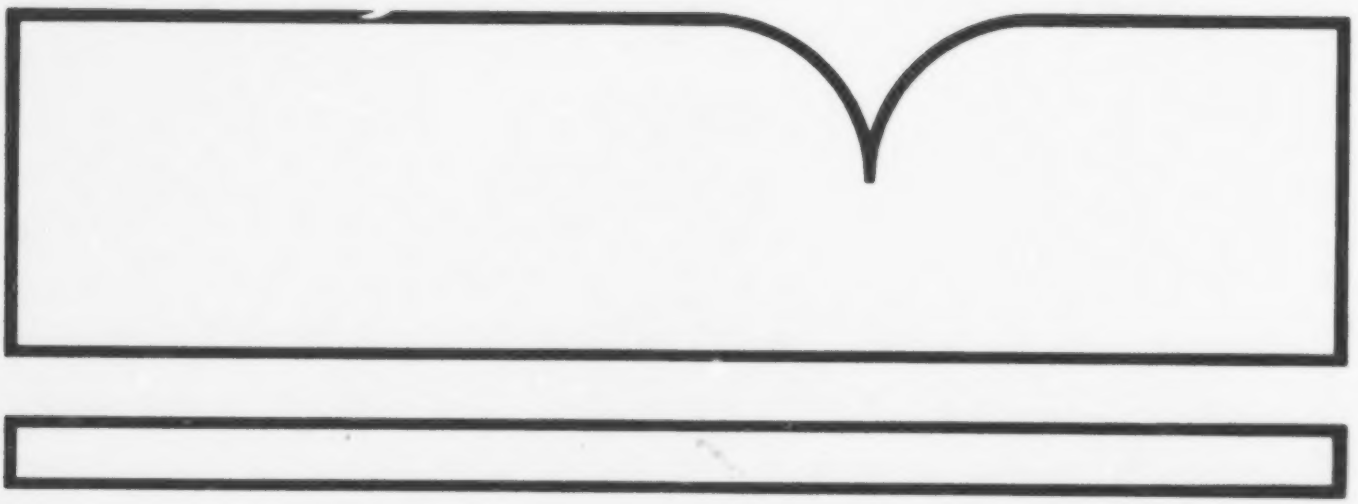

U.S. Department of Commerce
National Technical Information Service
NTIS

TECHNICAL REPORT DATA
(Please read Instructions on the reverse before compl

1. REPORT NO. EPA-600/J-81-184	2. Journal Article	PB82-153784
4. TITLE AND SUBTITLE USE OF WATER RAMAN EMISSION TO CORRECT AIRBORNE LASER FLUOROSENSOR DATA FOR EFFECTS OF WATER OPTICAL ATTENUATION		5. REPORT DATE December 1981 6. PERFORMING ORGANIZATION CODE 026039
7. AUTHOR(S) Michael Bristow, David Nielsen, Donald Bundy and Robert Furtek		8. PERFORMING ORGANIZATION REPORT NO.
9. PERFORMING ORGANIZATION NAME AND ADDRESS Environmental Monitoring Systems Laboratory Office of Research and Development U.S. Environmental Protection Agency Las Vegas, Nevada 89114		10. PROGRAM ELEMENT NO. 11. CONTRACT/GRANT NO.
12. SPONSORING AGENCY NAME AND ADDRESS U.S. Environmental Protection Agency--Las Vegas, NV Office of Research and Development Environmental Monitoring Systems Laboratory Las Vegas, Nevada 89114		13. TYPE OF REPORT AND PERIOD COVERED Journal Reprint 14. SPONSORING AGENCY CODE EPA/600/07

15. SUPPLEMENTARY NOTES

Reprinted from Applied Optics, Vol. 20, page 2889, September 1, 1981

16. ABSTRACT

Airborne laser fluorosensor measurements of fluorophore concentrations in surface waters are highly sensitive to interference from changes in optical attenuation. This interference can be eliminated by normalizing the fluorescence signal with the concurrent water Raman signal. In our application to remotely monitor chlorophyll a concentrations in fresh waters, the Raman-corrected chlorophyll a fluorescence measurements were found to be highly correlated with chlorophyll a ground truth data. Also, the reciprocal of the water Raman signal was seen to vary directly as the beam attenuation coefficient. It is suggested that this latter relationship be exploited as a means for remotely sensing changes in the optical attenuation of surface waters.

17. KEY WORDS AND DOCUMENT ANALYSIS

a. DESCRIPTORS	b. IDENTIFIERS/OPEN ENDED TERMS	c. COSATI Field/Group

18. DISTRIBUTION STATEMENT RELEASE TO PUBLIC	19. SECURITY CLASS *(This Report)* UNCLASSIFIED	21. NO. OF PAGES 20
	20. SECURITY CLASS *(This page)* UNCLASSIFIED	22. PRICE

EPA Form 2220-1 (Rev. 4-77) PREVIOUS EDITION IS OBSOLETE

TECHNICAL REPORT DATA
(Please read Instructions on the reverse before compl

1. REPORT NO. EPA-600/J-81-184	2. Journal Article	PB82-153784
4. TITLE AND SUBTITLE USE OF WATER RAMAN EMISSION TO CORRECT AIRBORNE LASER FLUOROSENSOR DATA FOR EFFECTS OF WATER OPTICAL ATTENUATION		5. REPORT DATE December 1981 6. PERFORMING ORGANIZATION CODE 026039
7. AUTHOR(S) Michael Bristow, David Nielsen, Donald Bundy and Robert Furtek		8. PERFORMING ORGANIZATION REPORT NO.
9. PERFORMING ORGANIZATION NAME AND ADDRESS Environmental Monitoring Systems Laboratory Office of Research and Development U.S. Environmental Protection Agency Las Vegas, Nevada 89114		10. PROGRAM ELEMENT NO. 11. CONTRACT/GRANT NO.
12. SPONSORING AGENCY NAME AND ADDRESS U.S. Environmental Protection Agency--Las Vegas, NV Office of Research and Development Environmental Monitoring Systems Laboratory Las Vegas, Nevada 89114		13. TYPE OF REPORT AND PERIOD COVERED Journal Reprint 14. SPONSORING AGENCY CODE EPA/600/07

15. SUPPLEMENTARY NOTES

Reprinted from Applied Optics, Vol. 20, page 2889, September 1, 1981

16. ABSTRACT

Airborne laser fluorosensor measurements of fluorophore concentrations in surface waters are highly sensitive to interference from changes in optical attenuation. This interference can be eliminated by normalizing the fluorescence signal with the concurrent water Raman signal. In our application to remotely monitor chlorophyll a concentrations in fresh waters, the Raman-corrected chlorophyll a fluorescence measurements were found to be highly correlated with chlorophyll a ground truth data. Also, the reciprocal of the water Raman signal was seen to vary directly as the beam attenuation coefficient. It is suggested that this latter relationship be exploited as a means for remotely sensing changes in the optical attenuation of surface waters.

17. KEY WORDS AND DOCUMENT ANALYSIS

a. DESCRIPTORS	b. IDENTIFIERS/OPEN ENDED TERMS	c. COSATI Field/Group

18. DISTRIBUTION STATEMENT RELEASE TO PUBLIC	19. SECURITY CLASS *(This Report)* UNCLASSIFIED	21. NO. OF PAGES 10
	20. SECURITY CLASS *(This page)* UNCLASSIFIED	22. PRICE

EPA Form 2220-1 (Rev. 4-77) PREVIOUS EDITION IS OBSOLETE

EPA-600/J-81-184
Journal Article

Reprinted from **Applied Optics**, Vol. 20, page 2889, September 1, 1981

Use of water Raman emission to correct airborne laser fluorosensor data for effects of water optical attenuation

Michael Bristow, David Nielsen, Donald Bundy and Robert Furtek

Airborne laser fluorosensor measurements of fluorophore concentrations in surface waters are highly sensitive to interference from changes in optical attenuation. This interference can be eliminated by normalizing the fluorescence signal with the concurrent water Raman signal. In our application to remotely monitor chlorophyll *a* concentrations in fresh waters, the Raman-corrected chlorophyll *a* fluorescence measurements were found to be highly correlated with chlorophyll *a* ground truth data. Also, the reciprocal of the water Raman signal was seen to vary directly as the beam attenuation coefficient. It is suggested that this latter relationship be exploited as a means for remotely sensing changes in the optical attenuation of surface waters.

I. Introduction

During the last decade, a considerable research effort has been directed toward development of a compact, lightweight, and reliable airborne laser fluorosensing device for monitoring water quality parameters. At present, the principal applications for this remote sensing technique are the identification of crude and refined petroleum oil-based substances distributed as surface water slicks[1-3] and measurement of the concentration of fluorophores (fluorescent substances) that are dispersed throughout the water column, such as phytoplanktonic chlorophyll *a*.[4-6] The latter class of application, involving vertically distributed fluorophores, is the subject of this study.

Airborne laser fluorosensors employ downward-looking pulsed lasers to induce fluorescence in a specific substance or group of substances distributed in the surface water volume, as illustrated in Fig. 1. The intensity of the fluorescence signal, to be used as a direct measure of the concentration of the fluorophore, is collected by a large aperture telescope and converted into an electrical signal using a photodetector.

Problems with this technique exist because of large variations in the penetration depth of the laser beam at sample points a short horizontal distance apart. These variations are produced by changes in the optical attenuation properties of surface waters caused, in turn, by variations in the concentration of either the fluorophore under investigation or other substances such as suspended sediments and dissolved organics. The net effect of this interference is that the fluorescence signal no longer varies simply as the concentration of the fluorophore, but is also strongly dependent on changes in the optical attenuation coefficients for the sample volume at the laser and fluorescence wavelengths.

The purpose of this study is to show how this problem can be eliminated by using the concurrent laser-induced water Raman emission to monitor changes in the penetration depth of the laser beam. The relatively intense backscattered signal from the O-H vibrational stretching mode of liquid water is, to a good approximation, dependent solely on changes in the optical attenuation coefficients. By taking the ratio of the intensities for the fluorescence signal from the fluorophore to that for the concurrent water Raman signal, a new parameter is obtained that is linearly dependent on the fluorophore concentration and essentially independent of changes in the optical attenuation coefficients for the sampled volume. Experimental data from a series of airborne laser fluorosensor measurements to monitor the concentration of phytoplanktonic chlorophyll *a* show that a significant improvement in the degree of correlation between the airborne and ground truth data is achieved when the airborne fluorescence data are corrected in this manner.

The authors are with U.S. Environmental Protection Agency, Environmental Monitoring Systems Laboratory, P.O. Box 15027, Las Vegas, Nevada 89114.

Received 20 March 1981.

II. Theory

The problem and its solution are best discussed in terms of the laser fluorosensor equation.[7–11] The formulation derived by Browell[11] is used here and gives the concentration of the vertically distributed fluorophore n_f in terms of measured, system, and environmental factors:

$$n_f = \left(\frac{P_F H^2}{P_L}\right)\left(\frac{4\pi\Delta_F}{T\eta_{tr}\eta_{rec}}\right) \times \left\{\frac{\mu_w^2 \exp[H(\beta_L + \beta_F)]}{(1 - R_w)^2}\right\}\left(\frac{k_L + k_F}{\sigma_f}\right) \cdot \text{mg/m}^3, \quad (1)$$

where P_F = peak detected fluorescence emission power at fluorescence wavelength F, W;
P_L = peak detected laser output power at laser wavelength L, W;
H = distance from sensor to fluorescent target, m;
T = effective collection area of telescope receiver, m^2;
Δ_F = ratio of fluorescence emission bandwidth to effective filter bandwidth, with a minimum value of 1;
η_{tr} = laser (transmitter) efficiency;
η_{rec} = telescope (receiver) efficiency;
R_w = specular reflectance for air–water interface at normal incidence for visible spectrum;
μ_w = refractive index of water for visible spectrum;
β_L = atmospheric beam attenuation coefficient at laser wavelength L, m^{-1};
β_F = atmospheric beam attenuation coefficient at fluorescence wavelength F, m^{-1};
k_L = effective attenuation coefficient for water at laser wavelength L, m^{-1};
k_F = effective attenuation coefficient for water at fluorescence wavelength F, m^{-1}; and
σ_f = effective *in vivo* fluorescence cross section for the fluorophore (chlorophyll *a*) for complete fluorescence band centered at wavelength F when excited at laser wavelength L, m^2/mg.

Factors within the first set of parentheses in Eq. (1) are calculated directly from each laser fluorosensor record obtained for a given sampling site. Those within the second set of parentheses are known or measurable laser fluorosensor system constants, and those within the third set of parentheses relate to known environmental factors. However, it is the difficulty in establishing values for the environmental factors within the fourth set of parentheses, specifically k_L and k_F, that constitutes the major limitation to the implementation of this remote-sensing technique. The assumptions made during the derivation of Eq. (1), in particular those regarding the parameters σ_f, k_F, and k_L, are discussed briefly below.

(1) It is assumed that contributions from the steady sky and solar background (both backscattered and specularly reflected) have been subtracted from the detected signal to obtain P_F.

(2) The surface water excitation volume is assumed to lie completely within the telescope field of view.

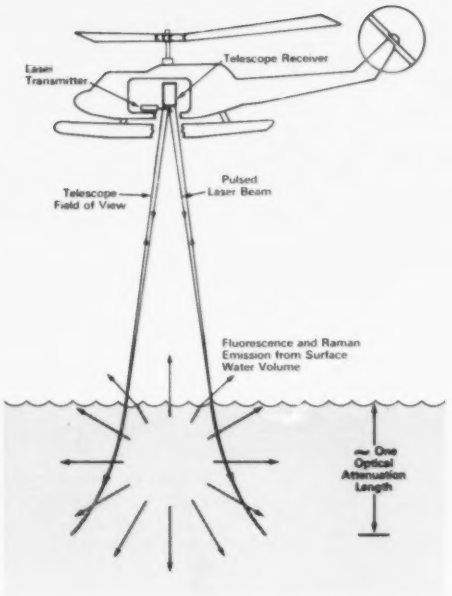

Fig. 1. Principle of operation of airborne laser fluorosensor. Not to scale.

(3) The fluorescence signal P_F is derived by integrating the incremental emission to infinite depth. This requires that the total depth of water being interrogated be at least an order of magnitude larger than the characteristic attenuation length represented by either k_F^{-1} or k_L^{-1}, whichever is the larger.

(4) Also inherent in the integration of the incremental fluorescence emission to derive P_F is the assumption that, at a given sampling site, n_f, k_L, k_F, and σ_f all remain constant with depth. For productive fresh and coastal waters, it is considered likely that mixing induced by wind and surface currents maintains the homogeneity of the surface layers. Although not justifiable on a theoretical basis, much published data exists,[12–15] suggesting that optical attenuation, as manifested by the beam attenuation coefficient α, remains essentially constant for at least the first two attenuation lengths given by $2\alpha^{-1}$. Further, by assuming that the effective attenuation lengths at the fluorescence and laser wavelengths, represented, respectively, by k_F^{-1} and k_L^{-1}, are on the same order of magnitude, it is not difficult to show that $(1 - 1/e^2)$ or 86.5% of the integrated fluorescence emission collected by the airborne sensor emanates from the sample volume defined by the first effective attenuation length.[10] Similarly, $(1 - 1/e^4)$ or 98.2% of the integrated fluorescence emission emanates from the first two effective attenuation lengths.

(5) The assumption is made that the fluorescence lifetime for the fluorophore is significantly less than the laser pulse width. In the present case, with a laser pulse width of about 250 nsec and an *in vivo* chlorophyll *a* fluorescence lifetime of less than 1 nsec,[16] this condition is clearly met.

(6) For clear atmospheric conditions in the visible part of the spectrum and over limited ranges on the

order of several hundred meters, the atmospheric attenuation term $\exp[H(\beta_L + \beta_F)]$ remains essentially constant with a value close to unity, so that the terms within the third set of parentheses can be treated as constants.

(7) The fluorophore fluorescence cross section σ_f is assumed to remain constant with change in horizontal location. In the present application, this condition requires that the percentage proportions of the different algal divisions (or color groups) that make up the phytoplankton community remain constant with horizontal location, because considerable variability exists between the values of σ_f for the different algal color groups.[4,10,17,18]

(8) Similarly, the effective attenuation coefficients k_L and k_F are assumed to remain constant with change in horizontal location and to be independent of the fluorophore (chlorophyll *a*) concentration n_f.

Even if σ_f, k_L, and k_F remain constant in both the horizontal and vertical dimensions, the determination of values for these parameters is not a straightforward proposition. Accurate values for σ_f can be obtained only by making careful and time-consuming *in situ* measurements concurrent with an airborne mission, an expedient that is clearly not practical when performing routine surveys.

With a sufficiently narrow laser pulse (~5 nsec), it is possible to obtain airborne measurements of k_F and k_L by monitoring the returned fluorescence and laser backscatter signals as a function of depth, provided that σ_f, k_F, and k_L remain constant over the first two attenuation lengths and that the receiver can adequately time resolve the signal this same depth interval. In airborne lidar bathymeter measurements made in waters off the Florida coast, Kim[19] used this approach to measure k_L by monitoring the bottom return from different depths on the assumption that bottom reflectivity remained constant and that k_L remained constant in the vertical dimension. The results showed that k_L was approximately five times smaller than the concurrent ground truth measurements of α. *In situ* measurements performed by Shannon[20] and Ofelt[21] have shown that the diffuse attenuation coefficient K and α can be related by the empirical relationship $K = 0.2\alpha + 0.04$ for the 530-nm wavelength region and for α less than 2 m^{-1}. This suggests that k relevant to the airborne lidar bathymeter application is closely related to K.

However, Kim[19] has also shown that k approaches K only when the angular field of view (FOV) of the receiver is sufficiently large that the receiver is able to intercept the bottom return component that is multiply scattered in the water column in addition to that for the unscattered bottom reflection, particularly in deep water where significant beam spreading occurs. As the FOV is reduced, less of the bottom return that is both singly and multiply scattered in the water column is intercepted by the receiver, and, in the limit of a vanishingly small FOV, the received signal is composed of a strong specular surface reflection and a weak bottom reflection. The intensity of the bottom reflection is then governed by α.

In the case of the laser fluorosensor, the receiver FOV is usually arranged to be on the same order as that defined by the laser spot on the water surface to minimize the amount of (solar) background radiation received by the detector when monitoring the relatively weak fluorescence signal. Restricting the receiver FOV is acceptable in this case because, as already indicated, the bulk of the integrated fluorescence return is emitted from the first attenuation length, which involves minimal spreading of the laser beam. This is in contrast to the bottom return signal received by the lidar bathymeter which may have traversed many attenuation lengths of water column, involving significant spreading of the laser beam. The intensity of that fraction of the received fluorescence signal that results from scattering of either the incident laser beam or the resultant fluorescence emission is then less than would be collected using a receiver with an extended FOV. In this situation, values for k will lie somewhere between those for K and α.

Unfortunately, laser pulse width and temporal resolution constraints do not allow for making airborne measurements of k_L and k_F with the laser fluorosensor employed in this study. In addition, because of the uncertainties introduced by the use of a receiver with a restricted FOV, the relationships between k and K or between k and α are not known. However, as will be shown, neither numerical data nor a theoretical model are required to describe the effective attenuation coefficient for the laser fluorosensor application when the Raman correction method is used to account for changes in these coefficients.

As a result of the problems in establishing values for σ_f, k_L, and k_F, an approach was initially adopted that assumes that the factors within the second, third, and fourth sets of parentheses in Eq. (1) remain constant but are unknown. Equation (1) can then be simplified to the form

$$n_f = C_1 P_F, \tag{2}$$

where P_F has been corrected for variations in P_L and H. Values for the constant C_1 are then obtained on the occasion of each airborne mission by making ground truth measurements for n_f at a small number of selected reference sites under the aircraft flight path concurrent with the airborne measurements of P_F.

Earlier flight tests of the laser fluorosensor indicated that the poor correspondence between n_f and P_F was due to significant changes in optical attenuation between sampling sites.[22] *In situ* measurements of the beam attenuation coefficient α for the red spectral region concurrent with the overflights indicated a fourfold increase in this parameter along the sensor flight path.[22] Values for the beam attenuation coefficient were also highly correlated with the corresponding extracted chlorophyll *a* data indicating that, in this specific circumstance, changes in optical attenuation (due to both absorption and scattering) were produced by changes in phytoplankton density rather than by changes in concentration of either nonchlorophyllous particulates

or dissolved materials. In addition to changes that occur over large distances, small scale horizontal variability in the water optical attenuation properties due to phytoplankton patchiness also contributes to this problem. In an extreme situation where attenuation is due solely to the presence of phytoplankton and all other loss sources become negligible, both k_F and k_L will be directly proportional to n_f with the result that the measured term $(P_F H^2/P_L)$ in Eq. (1) will remain constant regardless of changes in n_f. In the other extreme, where attenuation is dominated by nonchlorophyllous materials, large variations that occur in the measured values of $(P_F H^2/P_L)$ will bear little relationship to changes in n_f, the fluorophore concentration.

A solution to this problem has been proposed[22,23] whereby the concurrent laser-induced Raman emission from the 3418-cm^{-1} O-H vibrational stretching mode of liquid water is used as an indicator of changes in optical attenuation. For example, when excited at 470 nm, water Raman emission occurs at 560 nm as illustrated by the imaginary emission spectrum in Fig. 2. This spectrum, typical of many fresh and coastal waters, exhibits, in addition to the water Raman and chlorophyll *a* fluorescence bands, a relatively broad and intense fluorescence band that originates principally from dissolved organic substances.[24] As this Raman emission is a property of water alone, whose concentration n_w is a constant for all but grossly polluted effluents, the intensity of this relatively narrowband signal, as monitored by an airborne laser fluorosensor, will depend solely on the effective attenuation coefficients at the laser and Raman wavelengths, respectively, k_L and k_R. The effects of temperature[25] and salinity,[26] which are known to modify the shape of this emission band, do not significantly influence the integrated intensity of the whole band.

An equation analogous to Eq. (1) can be written that gives the peak-detected water Raman emission power P_R, in terms of measured, system, and environmental factors, such that:

$$P_R = \left(\frac{P_L}{H^2}\right)\frac{n_w \sigma_w d_R}{(k_R + k_L)}, \tag{3}$$

where σ_w is the Raman emission cross section for the O-H vibrational stretching mode of liquid water. σ_w is weakly dependent on temperature[25] and salinity[26] and exhibits a $1/\lambda_L^4$ dependence on the excitation wavelength λ_L, but, for a fixed laser wavelength and over a limited temperature range (5–25°C) in fresh waters, it is assumed to remain constant. d_R is dependent on known system and environmental factors and is given by the expression

$$d_R = \left(\frac{T\eta_{tr}\eta_{rec}}{4\pi\Delta_R}\right)\left\{\frac{(1-R_w)^2}{\mu_w^2 \exp[H(\beta_L + \beta_R)]}\right\}, \tag{4}$$

where Δ_R is the ratio of Raman emission bandwidth to the effective filter bandwidth, with a minimum value of 1, and β_R is the atmospheric attenuation coefficient at the Raman wavelength. All other terms are as defined for Eq. (1). For clear atmospheric conditions over paths of the order of 300 m, the term $\exp[H(\beta_L + \beta_R)]$ is assumed to have a value that remains close to unity, so that d_R can be treated as a constant.

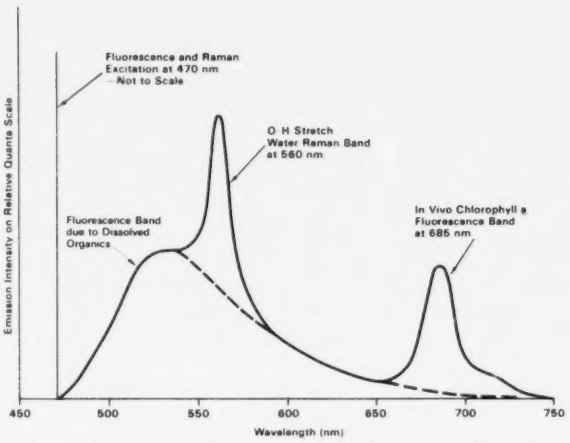

Fig. 2. Schematic showing spectral emission features typical of many fresh and marine waters produced by excitation at 470 nm.

A similar expression for the peak detected fluorescence emission power is obtained by rearranging Eq. (1) so that

$$P_F = \left(\frac{P_L}{H^2}\right)\frac{n_f \sigma_f d_F}{(k_F + k_L)}, \tag{5}$$

where

$$d_F = \left(\frac{T\eta_{tr}\eta_{rec}}{4\pi\Delta_F}\right)\left\{\frac{(1-R_w)^2}{\mu_w^2 \exp[H(\beta_L + \beta_F)]}\right\} \tag{6}$$

and is considered to be constant for the same reasons as given for d_R. An expression can now be written for the ratio P_F/P_R using Eqs. (3) and 5 that takes the form

$$\left(\frac{P_F}{P_R}\right) = \frac{n_f \sigma_f d_F}{n_w \sigma_u d_R}\left(\frac{k_R + k_L}{k_F + k_L}\right). \tag{7}$$

As n_w, σ_w, σ_f, d_R, and d_F are all considered to be constant, a new simplified expression for P_F/P_R is obtained:

$$\left(\frac{P_F}{P_R}\right) = n_f \delta\left(\frac{k_L + k_R}{k_L + k_F}\right), \tag{8}$$

where

$$\delta = \left(\frac{d_F \sigma_f}{d_R n_w \sigma_w}\right)$$

is a constant.

The ratio P_F/P_R is now dependent on n_f and the ratio $(k_L + k_R)/(k_L + k_F)$, but is independent of a number of parameters including laser power P_L, target range H, sensor efficiency factors that are the same for both P_F and P_R, and water surface reflectivity R_w; small changes in reflectivity can be expected as a result of wave action, whereas more significant changes are produced by off-nadir operation of the laser fluorosensor. Clearly, for Eq. (8) to be useful for determining values of n_f from airborne measurements of P_F/P_R, the ratio $(k_L + k_R)/(k_L + k_F)$ must remain constant or, at the most, change only slowly for significant changes in k_L, k_R, and k_F. For a given water body in which dissolved and partic-

ulate materials change only in concentration but not in character, it is, for the time being, assumed that the spectrum for k changes in amplitude but not in shape. Under these circumstances, $(k_L + k_R)/(k_L + k_F)$ will remain constant, independent of changes in k_L, k_R, and k_F. Further discussion of this subject is presented in Sec. V.A.

Assuming $(k_L + k_R)/(k_L + k_F)$ remains constant, Eq. (8) can be rearranged and simplified to the form

$$n_f = C_2\left(\frac{P_F}{P_R}\right). \tag{9}$$

where a value for the proportionality constant C_2 is established in the same manner as for C_1 in Eq. (2). It is significant that this expression is independent of variations in both laser power and target range and requires no information concerning either the theoretical form or the numerical values for the effective attenuation coefficients.

A preliminary airborne laser fluorosensor experiment[5] to evaluate the potential of this Raman normalization technique has been conducted over Lake Mead, Nevada, using laser excitation at 470 nm with corresponding water Raman emission at 560 nm. Results of these measurements showed that P_F/P_R provided a better indication of changes in chlorophyll a concentration than did P_F, thereby confirming the general correctness of the assumptions made in deriving Eq. (9). However, the chlorophyll a concentration varied over only a 2:1 range across the extent of the water body surveyed by the airborne laser fluorosensor and, as such, did not constitute a rigorous test of the validity of Eq. (9).

It is noteworthy that the measurements made at 560 nm in both the preliminary study[5] and the present study were actually for the total emission intensity at this wavelength rather than for the water Raman contribution alone. As illustrated by the imaginary spectrum in Fig. 2, the water Raman emission at 560 nm is superimposed on a relatively strong broadband fluorescence emission signal because of the presence of dissolved organics. In a separate study,[24] it has been shown that the amplitude of this organics-related fluorescence emission remains essentially constant over the extent of Lake Mead. This means that, in this particular circumstance, the total emission intensity at 560 nm can be used to correct the chlorophyll a fluorescence emission at 685 nm for attenuation effects without having to separate the Raman and fluorescence emission contributions at 560 nm. However, for most water bodies this organics-related fluorescence exhibits significant variability.[24,27] In situations such as these, it then becomes necessary to isolate the Raman component from the background fluorescence component by making two extra spectral measurements on either side of the Raman band and calculating the intensity of the Raman component by linear interpolation.

It should be mentioned that any residual problems involving changes in the ratio $(k_L + k_R)/(k_L + k_F)$ due to large changes in k_L, k_R, and k_F can be avoided by tuning the wavelength of the laser excitation source so that the wavelength of the Raman band becomes coincident with that for the fluorescence band under investigation. In these conditions, k_R becomes equivalent to k_F, so that $(k_L + k_R)/(k_L + k_F) = 1$. However, this expedient is only practical for those situations where the fluorescence band is considerably broader than the water Raman band, so that their respective contributions at the common wavelength are easily separable by interpolation. Unfortunately, when the water Raman band is tuned into coincidence with the chlorophyll a fluorescence band at 685 nm, using excitation at 555 nm, the width of the water Raman band (~20 nm) is on the same order as that for the chlorophyll a fluorescence band. Clearly, separation of the fluorescence and Raman emission contributions at this common wavelength would not be straightforward. An acceptable compromise can probably be achieved by tuning spectrally the Raman band a short interval to the short wavelength side of the fluorescence band, such that the dependence of $(k_L + k_R)/(k_L + k_F)$ on the individual k values remains negligibly small for all but the largest changes in attenuation.

III. Instrumentation

As a detailed description of the airborne laser fluorosensor system has been given by Bristow *et al.*,[5,22] only a brief description is presented here.

The laser fluorosensor consisted of a laser transmitter and a telescope receiver, which were mounted in a lightweight aluminum box structure in a noncoaxial configuration as shown by the side view schematic in Fig. 3. The system was installed on a Bell UH 1D/H (Huey) helicopter with the transmitter/receiver module centrally positioned over a clear hole cut between two stringers just forward of the transmission housing. The system was operated in a fixed downward-looking mode, which, at a laser repetition rate of 1 pulse/sec (pps) and a typical aircraft ground speed of 30 m/sec, gave a ground footprint spacing of 30 m. At an above-target elevation of 300 m, the laser beam divergence of 6 mrad produced a water surface spot diameter of 1.8 m.

A. Laser Transmitter

The coaxial flashlamp-pumped dye laser (Phase R DL-1200) emits pulses of 200-kW peak power and 250-nsec full width at half-maximum (FWHM) at a repetition rate of 1 pps. Stable and relatively long-life laser performance at 470 nm was achieved using coumarin 311 laser dye[28] in methanol. The peak laser power was monitored by directing a small fraction of the laser output onto a calibrated PIN silicon photodiode via a quartz diffuser plate. The laser power signal was also used to trigger the oscilloscope and the waveform digitizer and to initiate operation of a delayed pulse generator used to control the electronics for gating the two photomultipliers. Wavelength tuning of the laser using a single prism dispersing element was performed at the beginning of each flight by maximizing the detected water Raman emission signal as monitored through a narrowband interference filter centered at 560 nm. The tuned laser output at 470 nm had a spectral

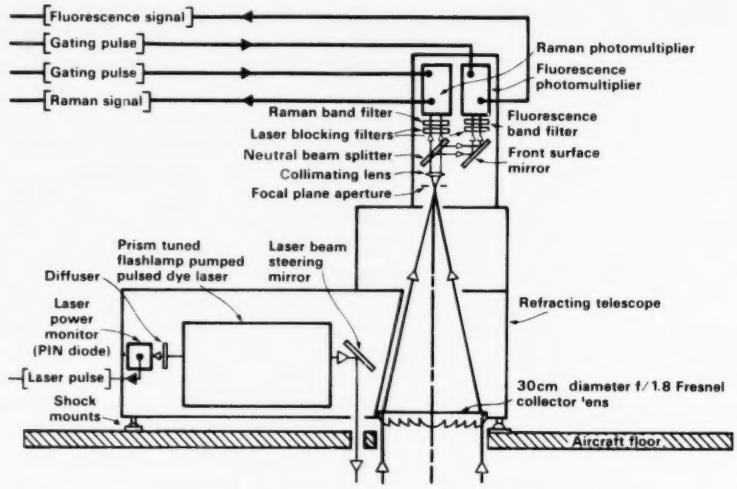

Fig. 3. Optical diagram of airborne laser fluorosensor for monitoring chlorophyll *a* fluorescence and water Raman signals.

bandwidth of 0.8 nm at FWHM, which is sufficiently narrow that the water Raman emission at 560 nm exhibits its true limiting (FWHM) bandwidth of 13.5 nm for this wavelength.[25]

B. Selection of Laser Excitation Wavelength

Choice of excitation at 470 nm rather than at 440 nm as previously used[5,22] was a compromise reached after consideration of a number of conflicting factors. Reasons for preferring excitation in the blue-green (~500 nm) region rather than in the violet (~440 nm) region are:

(1) In order that the ratio $(k_L + k_R)/(k_L + k_F)$ be independent of changes in the individual k values, the water Raman emission band should be tuned as closely as possible to the shortwavelength side of the chlorophyll *a* fluorescence band without causing overlap between the two bands. With excitation at 500 nm, the water Raman band is centered at 603 nm, thereby ensuring adequate separation of the two emission bands, while, at the same time, minimizing differential spectral attenuation effects.

(2) Flash lamp excited laser dyes for operation in the blue-green region, such as coumarin 311, have been found to be more efficient and durable than dyes, such as coumarin 120, that operate in the violet region close to 440 nm.

(3) The background fluorescence signal at 685 nm (see Fig. 2) due to the presence of high concentrations of organics can constitute a significant source of interference in the chlorophyll *a* fluorescence measurements. A significant reduction in the intensity of this organics-related background fluorescence at 685 nm can be realized by shifting excitation to longer wavelengths.

(4) Because the wavelength of maximum optical transmission for most natural waters generally occurs in the blue-green region between 470 and 520 nm, excitation in this region is preferred to that in the violet region. This results in reduced attenuation of the laser beam in the surface water sample volume that, in turn, results in an increase in the signals (and SNRs) for the water Raman and chlorophyll *a* fluorescence returns, as predicted, respectively, by Eqs. (3) and (5).

(5) Phytoplankton from each of the principal fresh water algal color groups contain, with some exceptions, varying quantities of the various photosynthetic pigments, such that each group has its own peculiar excitation spectrum responsible for the characteristic chlorophyll *a* fluorescence emission at 685 nm. As a result, no single excitation wavelength exists that produces the same intensity of emission at 685 nm from equivalent samples of each of the different algal color groups likely to be encountered in most fresh and marine waters.[4,10,17,18] The excitation spectra for most fresh water algal color groups tend to be peaked in the blue-green spectral region because of absorption by chlorophyll *a* in the 440-nm region and by chlorophyll *b* and the carotenoid proteins in the 480-nm region. A notable exception to this behavior is the excitation spectrum for blue-green algae, which is dominated by a maximum in the 620-nm region because of the biliprotein, *c*-phycocyanin.[4,10,17,18] Examination of the cited literature on the excitation spectra of *in vivo* algal monocultures suggests that excitation in the 500-nm region constitutes the best compromise wavelength for achieving near uniform 685-nm fluorescence response in natural samples containing different phytoplankton mixtures but having the same chlorophyll *a* concentration.

In contrast to the above factors promoting longwave excitation, there are a number of factors calling for excitation at 440 nm or even shorter wavelength. These are:

(1) The intensity of the Raman emission exhibits a $1/\lambda_L^4$ dependent on the excitation wavelength λ_L such that shortwave excitation results in a significant increase in the Raman signal.

(2) Excitation at 440 nm produces water Raman emission at 518 nm, close to the wavelength for peak transmission in moderately productive waters.[29] This

results in reduced attenuation of the Raman emission that, in turn, results in an increase in the signal (and SNR) for the water Raman return, as predicted by Eq. (3).

(3) Excitation at 440 nm produces a significantly stronger fluorescence response from most (*in situ*) fresh water algal color types through direct absorption by chlorophyll *a*, than does excitation at 500 nm through absorption by a combination of accessory photosynthetic pigments. As already noted, blue-green algae are an exception to this behavior.

(4) As most photomultiplier detectors achieve their peak quantum efficiency in the near UV–violet spectral region, it is desirable to locate the water Raman band in this region to reduce the influence of in-signal (shot) photoelectron noise on laser fluorosensor performance.

(5) In a separate study,[24] it has been shown that the intensity of the Raman-normalized fluorescence signal due to dissolved organics, apparent in Fig. 2 as the relatively intense broad emission band peaked in the 530-nm region, is highly correlated with the dissolved organic carbon (DOC) content of a sample. Consequently, in those situations where it is intended to monitor remotely this organics-related fluorescence for use as a surface water DOC indicator concurrently with the chlorophyll *a* fluorescence signal, the DOC fluorescence emission can be maximized by exciting the sample at relatively shortwavelengths, preferably in the near UV.

C. Optical Receiver

The receiver consisted of an acrylic Fresnel lens (30-cm diam, *f*/1.8), a focal plane aperture, a collimating lens, a neutral (50/50) beam splitter, and two gated photomultipliers with their respective filters, as shown in Fig. 3. The Fresnel lens was chosen both for its low mass that requires a minimum of support structure and for its low cost. Although low *f*-number spherical refractors of this type produce large blur circles (circles of least confusion) at the focal plane, this effect did not constitute a significant problem in these experiments because of the relatively high power density of the laser pulse at the water surface in relation to the solar background power level.[22] The chlorophyll *a* fluorescence band was isolated with a 22-nm (FWHM) passband interference filter centered at 685 nm, with additional laser blocking provided by a longwave pass glass absorption filter (Corning 2-58) with a 50% cutoff point at 645 nm. Similarly the Raman band was isolated with a 10-nm (FWHM) passband interference filter centered at 560 nm, with additional laser blocking provided by a longwave pass glass absorption filter (Corning 3-69) with a 50% cutoff point at 520 nm.

Problems were initially encountered with both the interference and glass absorption type filters, which were found to be highly fluorescent in their respective passbands when exposed to the laser radiation specularly reflected from the water surface. This sometimes intense filter fluorescence was minimized to an acceptable level by choosing filters with low inherent fluorescence and by selectively orienting and positioning the interference and absorbing glass filters with respect to the incoming laser radiation.[30]

Neutral density attenuation filters were employed as necessary to ensure that the detected signal did not exceed the photomultiplier linearity limit. The fluorescence and Raman detectors were 5-cm diam 12-stage red sensitive (S-20 response) end-on photomultipliers (RCA C31000A). Saturation of the photomultipliers, caused by continuous exposure to the backscattered sky and solar background radiation, was avoided by gating-on the supply to dynodes 4, 6, and 8 for the duration of each fluorescence and Raman return signal,[22] thereby providing an on/off ratio of about 2000:1. In addition, gating the detectors also provided a measurement of the steady (DC) background current at the instant the fluorescence and Raman signals were measured. A determination could then be made to ensure that the photomultipliers had stayed in the linear operating region during the measurement of the fluorescence and Raman signals.

Because of the noncoaxial configuration of the laser and telescope, it was necessary to bring the image of the surface water laser excitation spot into coincidence with the telescope focal plane aperture for a given target range; the diameter of the focal plane aperture was chosen to be the same as that for the image of the surface water laser spot to minimize the solar background signal. This process was performed at the beginning of each flight for a prescribed range interval by making fine adjustments to the position of the laser spot on the water surface using the laser beam steering mirror shown in Fig. 3. Precise alignment of the image of the laser spot with the focal plane aperture was achieved by maximizing the amplitude of the detected water Raman signal at a location known to exhibit conditions of nearly constant optical attenuation.

D. Data Acquisition System

A schematic showing the elements of the data acquisition system, including the detector gating, monitoring, and recording subsystems, is shown in Fig. 4. Events were initiated by the laser power pulse which was used to trigger a monitoring oscilloscope. The oscilloscope time-base gate output was then used to trigger a pulse generator that, in turn, initiated formation of delayed detector-gating pulses. The delay period for these pulses was adjusted so that the detectors were activated several hundred nanoseconds before the anticipated arrival of the backscattered fluorescence and Raman signals. The series of events is conveniently illustrated by the oscillogram in Fig. 5, which shows the laser pulse together with the backscattered chlorophyll *a* fluorescence and water Raman signals superimposed on their respective solar background signals. The signal from the Raman detector was delayed by 3 μsec so that all three signals could be conveniently displayed and recorded on a single time base. In the example of Fig. 5 with an airborne target elevation of 255 m, the detectors were gated-on for a 2.5-μsec period after an initial 1-μsec delay. The solar background signal levels due

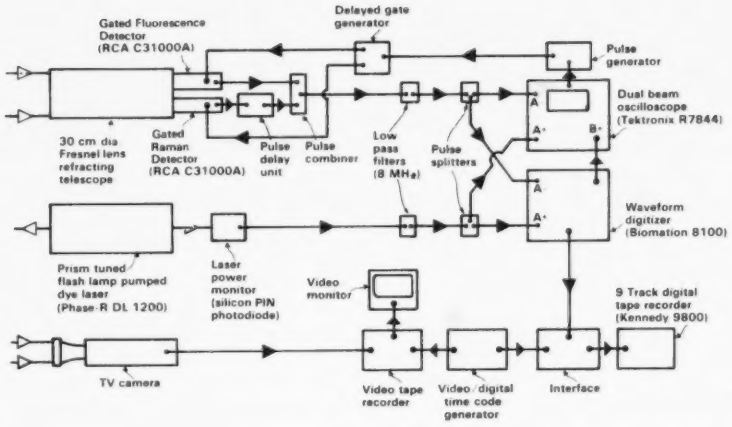
Gated Fluorescence Detector (RCA C31000A)
Delayed gate generator
Pulse generator
Dual beam oscilloscope (Tektronix R7844)
30 cm dia Fresnel lens refracting telescope
Gated Raman Detector (RCA C31000A)
Pulse delay unit
Pulse combiner
Low pass filters (8 MHz)
Pulse splitters
Waveform digitizer (Biomation 8100)
Prism tuned flash lamp pumped dye laser (Phase-R DL 1200)
Laser power monitor (silicon PIN photodiode)
Video monitor
9 Track digital tape recorder (Kennedy 9800)
TV camera
Video tape recorder
Video/digital time code generator
Interface

Fig. 4. Schematic of airborne laser fluorosensor for measuring chlorophyll *a* fluorescence and water Raman signals, showing elements of detection, monitoring, and recording systems.

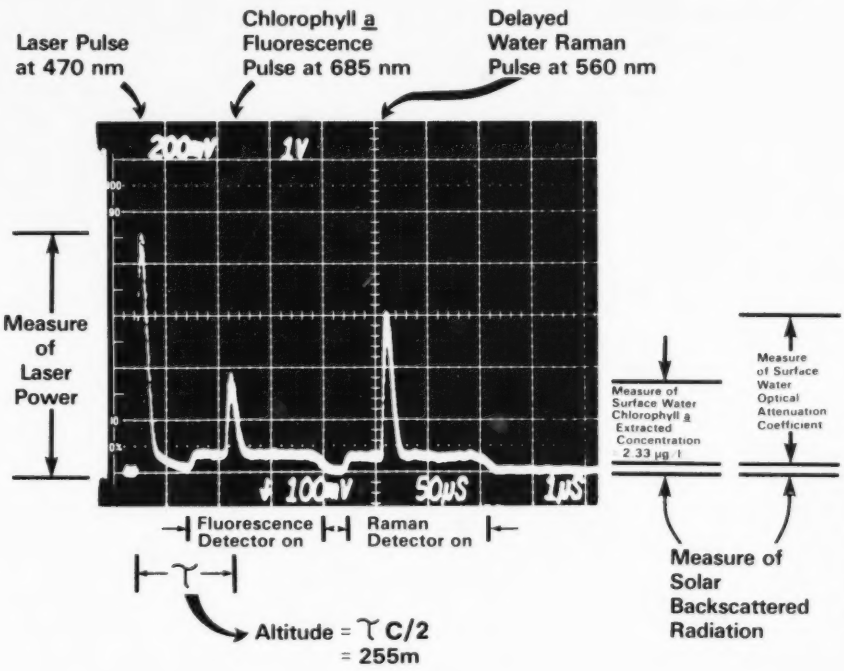
Laser Pulse at 470 nm
Chlorophyll a Fluorescence Pulse at 685 nm
Delayed Water Raman Pulse at 560 nm
200mV
1V
100mV
50μS
1μS
Measure of Laser Power
Fluorescence Detector on
Raman Detector on
τ
Altitude = τ C/2 = 255m
Measure of Surface Water Chlorophyll a Extracted Concentration 2.33 μg l
Measure of Surface Water Optical Attenuation Coefficient
Measure of Solar Backscattered Radiation

Fig. 5. Oscillogram showing time sequence of airborne laser fluorosensor signals obtained over buoy 11 in the Las Vegas Bay region of Lake Mead, Nevada on 24 Jan. 1979 for a measured chlorophyll *a* concentration of 2.33 μg/l.

to both sky and solar backscatter and to sky specular surface reflection components did not constitute a serious source of noise in these experiments. Problems with solar glitter were avoided by conducting the flights at times of relatively low sun angle.

These signal waveforms were also digitized into 512 channels, each 10-nsec wide with approximately 6-bit resolution using a fast waveform digitizer (Biomation 8100). These digitized waveforms were then recorded on magnetic tape using a 9-track tape recorder (Kennedy 9800). The effective signal bandwidth of the combined analog and digital electronics was 8 MHz, dictated principally by the low pass filters used to reduce the amplitude of photoelectron and electromagnetic noise. A computer plot of a typical digitized waveform is shown in Fig. 6.

Navigation, target evaluation, and track recovery were facilitated using a TV camera with a wide angle lens that was mounted directly to the laser fluorosensor module and bore-sighted with the laser beam. This allowed the helicopter flight path over a chosen water surface target to be viewed directly on a video monitor and also to be recorded on video cassette. To use this video recording to aid the interpretation of the laser fluorosensor data, a video/digital time-code generator was used to index each digital laser fluorosensor record and each video frame with a time signal to the nearest 1/100 sec. It was then possible to establish an approximate location for each laser fluorosensor record in relation to a series of marker buoys.

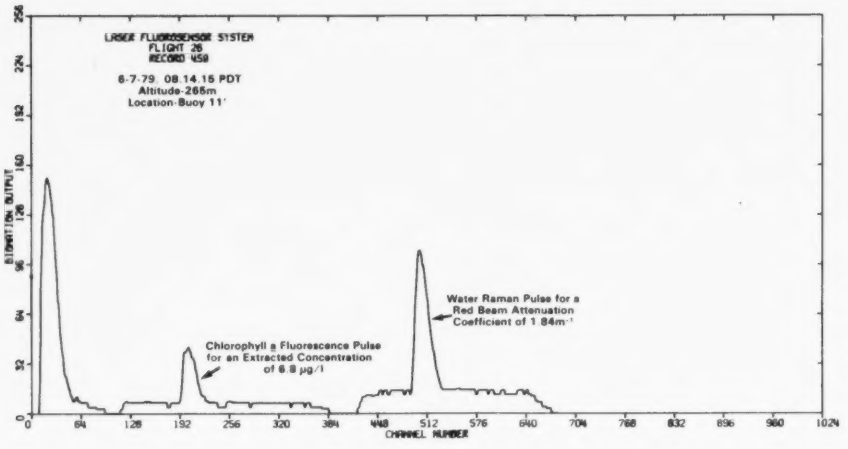
LASER FLUOROSENSOR SYSTEM
FLIGHT 26
RECORD #58
6-7-79 08.14.15 PDT
Altitude-265m
Location-Buoy 11'
Chlorophyll a Fluorescence Pulse for an Extracted Concentration of 6.8 µg/l
Water Raman Pulse for a Red Beam Attenuation Coefficient of 1.84m⁻¹
CHANNEL NUMBER

Fig. 6. Plot of digital laser fluorosensor record, showing time sequence of airborne laser fluorosensor signals obtained over buoy 11′ in the Las Vegas Bay region of Lake Mead, Nevada on 7 June 1979 for a measured chlorophyll *a* concentration of 6.8 µg/l.

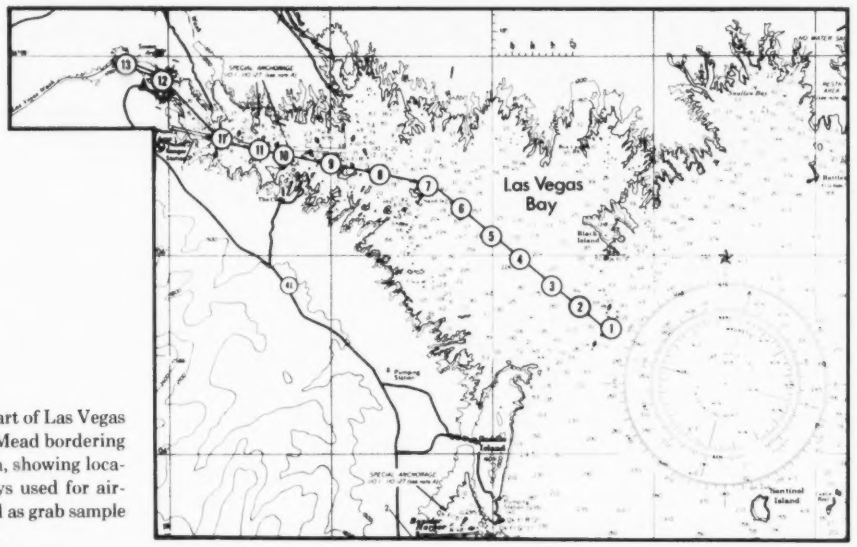

Fig. 7. Nautical chart of Las Vegas Bay region of Lake Mead bordering Nevada and Arizona, showing location of marker buoys used for airborne navigation and as grab sample sites.

IV. Field Tests

A. Description of Field Site and Ground Truth Measurements

Airborne testing and evaluation of the laser fluorosensor were made over the Las Vegas Bay region of Lake Mead. A nautical chart for this area is shown in Fig. 7. High concentrations of nutrients and other pollutants enter the western end of Las Vegas Bay from Las Vegas Wash, which is essentially an open stream carrying both partially treated and untreated wastewater from the city of Las Vegas. Ground truth support for these airborne measurements was performed by personnel of the Department of Biological Sciences at the U. Nevada–Las Vegas. This involved collecting samples from points at and halfway between 14 marker buoys located along the center line of Las Vegas Bay leading toward Las Vegas Wash. This line of buoys, shown in Fig. 7 and easily seen from a height of 300 m, was flown as three separate straight flight lines. The lengths of these lines from buoys 1 to 7, 7 to 11′, and 11′ to the shoreline are, respectively, 4452 m, 3544 m, and 2725 m. Not surprisingly, the highest chlorophyll *a* concentrations generally occurred in the shoreline region lying closest to the point where Las Vegas Wash enters Las Vegas Bay, whereas the lowest concentrations generally occurred at buoy 1.

Grab samples for laboratory chlorophyll *a* determinations were obtained at a 0.5-m depth at the time of the overflights from three equidistant locations on the circumference of an ~25-m diam circle around each sampling station. These three subsamples were then mixed to reduce the effects of small scale horizontal phytoplankton variability on the chlorophyll *a* determinations. In addition, the collection of samples at a finite distance from the buoys also minimized the chances of including in the subsamples significant amounts of periphyton that might break from the buoy surfaces.

Considerable attention was paid to improving the reliability and reproducibility of the chlorophyll *a*

ground truth determinations, particularly as these data are the standard against which the performance of the remote sensing device is gauged. In our experience, the reproducibility of chlorophyll *a* determinations in routine water quality work is often significantly lower than that of the raw data obtained using either active (laser) or passive (multispectral) remote sensing devices. However, it should be mentioned that interpretation of the remotely sensed data may introduce additional uncertainties into the calculated chlorophyll *a* concentration. For example, in the case of the laser fluorosensor, a likely source of this uncertainty involves the point-to-point variation in the *in vivo* chlorophyll *a* fluorescence cross section σ_f, which, for the purposes of this study, is assumed to be constant. The absolute value of σ_f for a given excitation wavelength is known to be critically dependent on a number of environmental factors[11,31–35] and also on the particular algal color groups present in the sample.[4,10,17,18] However, in spite of possible changes in σ_f, it is clear that the reproducibility of the chlorophyll *a* ground truth data must be at least as good as that of the corresponding remotely sensed chlorophyll *a* data.

In an attempt to remedy this situation, a separate investigation was conducted with the purpose of improving the reliability of the chlorophyll *a* determination procedure and, at the same time, of enhancing the efficiency by which chlorophyll *a* is extracted from the (fresh water) phytoplankton. The extraction efficiency depends critically on the extraction procedure and on the divisions and classes of phytoplankton present in the sample and almost never approaches 100%. An extraction procedure was adopted that demonstrated a significant improvement in efficiency and reproducibility over the standard procedure of Strickland and Parsons.[36] A description of this procedure together with the related analytical methodology is given by Furtek.[37] All samples were analyzed in triplicate according to this procedure, and the mean chlorophyll *a* value for each sample was then used for comparison with the corresponding airborne laser fluorosensor data.

In addition to the analysis of discrete samples, *in situ* measurements of the beam attenuation coefficient and *in vivo* chlorophyll *a* fluorescence were obtained at the time of the overflights in the form of continuous chart-recorded profiles corresponding to the laser fluorosensor flight path, as defined by the line of buoys shown in Fig. 7.

The beam attenuation coefficient was obtained using a 1-m path length transmissometer (Martek, Model XMS). This device measures beam transmittance T, which is related to the beam attenuation coefficient α through the familiar expression $T = \exp(-\alpha x)$, where $x(= 1\text{ m})$ is the optical path length of the beam. The transmissometer was mounted on a boom ahead of the survey launch at a 1-m depth to be able to record the attenuation of the undisturbed water ahead of the moving launch. The present measurements were made at a 610-nm wavelength using a 32-nm (FWHM) bandwidth filter.

The *in situ* fluorometry was performed using a field fluorometer (Turner Designs, Model 10) fitted with a high-volume continuous flow-through cuvette system. The entry port for the flow-through sampling tube was located directly adjacent to the optical path of the transmissometer to ensure a close correspondence between the samples for these two *in situ* sensors. The flow-through sample pump was located downstream of the fluorometer to avoid phytoplankton cell breakage or contamination of the sample by either cavitation bubbles or pump lubricant prior to passage of the sample through the cuvette. Sample excitation, nominally at 440 nm, was achieved using a blue fluorescent lamp in combination with Corning filters 5-60 and 3-73. The latter filter, a longwave pass type with a 50% cutoff point at 433 nm, was used to prevent excitation of the chlorophyll degradation product pheophytin *a*, which has an excitation spectrum that peaks in the 410-nm region and falls to near zero at 440 nm.[38] The effective center wavelength and (FWHM) bandwidth for this filter combination are 452 nm and 46 nm, respectively. The fluorescence emission at 685 nm was detected using a red sensitive (Hamamatsu R446) photomultiplier in combination with a Corning 2-64 longwave pass filter.

B. Analysis of the Airborne Data

Prior to analyzing each record, a check was performed to ensure that the peak signal levels from the fluorescence and Raman detectors, which include their respective solar background contributions, remained in the linear operating region at all times. It is possible, particularly when flying at times of high sun angle, for solar glitter to drive the photomultipliers into the nonlinear operating region or even into saturation.

The digital data for the laser, fluorescence, and Raman pulses, respectively P_L, P_F, and P_R, were analyzed according to area (pulse energy) rather than to pulse height (peak power) to gain the advantage of the noise reducing properties of the integration process. However, smoothing of the individual records to reduce the effect of in-signal and background noise on the analysis was not necessary in view of the good SNR of the received signals, as indicated by the records shown in Figs. 5 and 6. Pulse integration was performed over all time channels having signal counts greater than, say, 1/20th of the peak pulse count above background to avoid including background signal counts in the pulse signal.

The time domain centroids of the laser and fluorescence pulses were calculated for use in establishing a value for H, the distance between the sensor and the surface water fluorescent target. Although the widths at FWHM for the laser and fluorescence pulses were on the order of 250 nsec, it was found that the reproducibility of the H measurement could be made to a precision on the order of 1 m using this approach.

P_F and P_R were then corrected for variations in H and P_L by normalization to arbitrary constant values of target range and laser power. In the case of H, the normalization follows a $1/H^2$ dependence, whereas for

P_L, the normalization is made on the assumption that P_F is directly proportional to P_L. The values of P_R and P_F that are presented in Sec. V are therefore more correctly represented by the terms $(P_R H^2/P_L)$ and $(P_F H^2/P_L)$, respectively. The satisfactory nature of this normalization procedure was demonstrated by the fact that the respective profiles of P_F and P_R for the three separate legs that comprise the overall flight line between buoys 1 and 13 could be patched together in sequence without discontinuity even though the sensor was invariably flown at different target ranges and operated at different laser power levels during the coverage of each leg.

All profiles of P_F, P_R, and P_F/P_R were smoothed to reduce the amplitude of fluctuations due to system noise, due to changes in water surface reflectivity, and due to small scale horizontal patchiness in phytoplankton distribution, while leaving the large scale features unchanged. A moving 5-point average scheme was found to be satisfactory for this purpose. However, it should be noted that this smoothing procedure reduces the effective ground resolution of the airborne data. For example, at the laser repetition rate of 1 pps and at a typical helicopter ground speed of 30 m/sec, the ground resolution element of the unsmoothed airborne data is effectively 30 m in size, whereas that for the data smoothed by the 5-point averaging procedure is degraded to 150 m. This reduction in ground resolution for the airborne data was considered acceptable in the present situation because the ground truth data, against which the airborne data is to be compared, was obtained at sampling points that were separated by a mean distance of 383 m. Clearly, when performing routine airborne surveys, the nature of the sensor target and the spatial dimensions of the phenomena being investigated should be considered in conjunction with the aircraft ground speed and laser pulse repetition rate when deciding on whether or not to smooth the data or, if so, on the degree of smoothing to be applied.

As mentioned earlier, the output data from the airborne laser fluorosensor cannot be permanently calibrated in terms of chlorophyll a concentration because of the day-to-day variability in the chlorophyll a fluorescence cross section σ_f, because values for the effective attenuation coefficients k_L, k_F, and k_R are not available and because values for the system parameters appearing within the second set of parentheses in Eq. (1) are critically dependent on the state of adjustment of the laser fluorosensor at any given time. Rather, the sets of values that constitute the profiles of P_F and P_F/P_R were normalized to the corresponding set of values for the chlorophyll a ground truth data using the calibration constants C_1 [from Eq. (2)] and C_2 [from Eq. (9)], respectively. Values for these constants were calculated by minimizing the summed effect of the numerical differences between the values for the ground truth data and the corresponding values for P_F and P_F/P_R obtained over the ground truth sampling sites by means of the method of least squares. These constants were then used to bring the complete airborne profile into numerical coincidence with the corresponding ground truth profile. The particular laser fluorosensor records corresponding to the marker buoy sampling sites were obtained from the video recording of the sensor flight path. The exact location of the laser spot on the water surface was visible in most video records by virtue of the specular surface return of the laser pulse. Consequently, as each laser fluorosensor record and each video frame are time referenced to the nearest 1/100 sec, it was possible to identify the records corresponding to each of the marker buoy sampling sites.

V. Discussion

A. Raman Correction of Attenuation by Phytoplankton

Results of the airborne measurements conducted over the Las Vegas Bay flight line (Fig. 7) on 7 June 1979 are shown in Fig. 8 in the form of smoothed profiles of chlorophyll a fluorescence pulse energy P_F, water Raman pulse energy P_R, and P_F/P_R as functions of flight time. In addition, the location of the sampling sites and an approximate horizontal distance scale are indicated. Also shown in Fig. 8 are the ground truth measurements of the extracted chlorophyll a concentration n_f for the grab samples obtained at the 28 sampling sites at the time of the laser fluorosensor overflights. For the purpose of illustration, the values of n_f were normalized to the laser fluorosensor profile of P_F/P_R rather the converse, which would normally be the case as suggested in Sec. IV.B.

From Fig. 8, it is immediately apparent that P_F/P_R and the chlorophyll a data are highly correlated over the extent of the flight path. On the other hand, normalization of n_f to the uncorrected fluorescence signal P_F, which is not shown in Fig. 8, resulted in an extremely poor fit. This is not surprising as P_F varies over a range of ~4:1, whereas both P_F/P_R and n_f vary over a range of ~10:1.

A number of circumstantial factors unrelated to laser fluorosensor performance provided ideal conditions for performing these measurements. First, a relatively

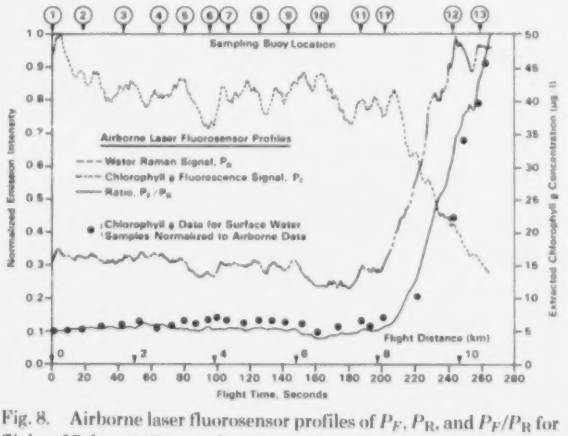
Sampling Buoy Location
Airborne Laser Fluorosensor Profiles
Water Raman Signal, P_R
Chlorophyll a Fluorescence Signal, P_F
Ratio, P_F/P_R
Chlorophyll a Data for Surface Water Samples Normalized to Airborne Data
Normalized Emission Intensity
Extracted Chlorophyll a Concentration (ug l)
Flight Distance (km)
Flight Time, Seconds

Fig. 8. Airborne laser fluorosensor profiles of P_F, P_R, and P_F/P_R for flight of 7 June 1979 over Las Vegas Bay. Profiles smoothed using a moving 5-point average scheme. Also shown are the chlorophyll a values for the 28 ground truth samples, which have been normalized to the laser fluorosensor profile for P_F/P_R.

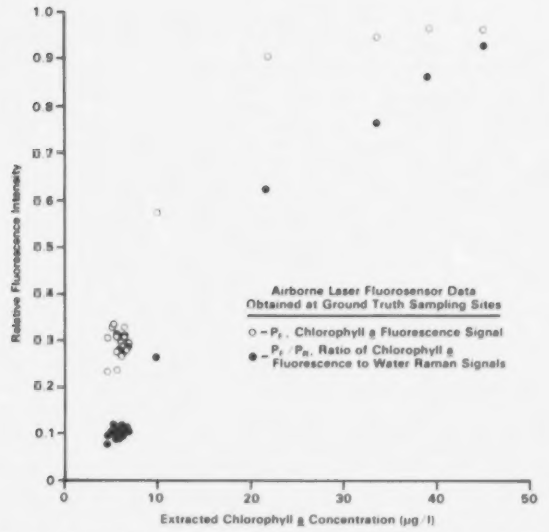
Airborne Laser Fluorosensor Data
Obtained at Ground Truth Sampling Sites
○ – P_F, Chlorophyll a Fluorescence Signal
● – P_F / P_R, Ratio of Chlorophyll a Fluorescence to Water Raman Signals
Relative Fluorescence Intensity
Extracted Chlorophyll a Concentration (μg / l)

Fig. 9. Dependence of P_F and P_F/P_R on chlorophyll a concentration n_f for the 28 sampling sites in Las Vegas Bay on 7 June 1979. Airborne data were taken from the smoothed laser fluorosensor profiles for P_F and P_F/P_R.

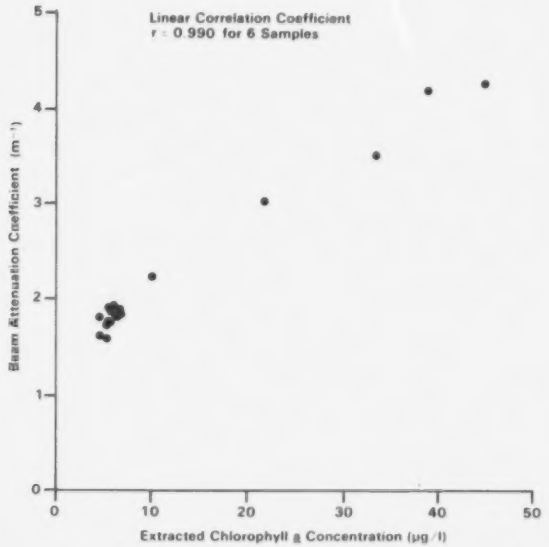
Linear Correlation Coefficient
r = 0.990 for 6 Samples
Beam Attenuation Coefficient (m⁻¹)
Extracted Chlorophyll a Concentration (μg / l)

Fig. 10. Variation of *in situ* measurement of beam attenuation coefficient with chlorophyll a concentration n_f for the 28 sampling sites in Las Vegas Bay on 7 June 1979. Correlation coefficient is based on 6 samples, one of which is the mean of the group of 23 samples near the origin.

strong (~20 knot) wind had the effect of significantly reducing the presence of small scale horizontal structure in the phytoplankton distribution, thereby reducing the requirement for precise navigation over the sampling buoys. Second, this wind-induced homogenization also reduced patchiness problems that would otherwise cause considerable variability between the three ground truth grab samples used for characterizing a given sampling site. Third, both the high values (~45 μg/l) and the large (10-times) overall change encountered in n_f provided an ideal opportunity for testing the water Raman correction method. Finally, as all chlorophyll a values encountered on this occasion were relatively high (4.6–45 μg/l), the random errors incurred in their determination from the grab samples should be relatively small.

The smoothed values of P_F and P_F/P_R that were obtained for the 28 ground truth sampling sites are plotted in Fig. 9 as a function of n_f. The highly nonlinear variation of P_F with n_f can best be explained by reference to Eq. (5). As n_f increases, k_F and k_L become more uniquely dependent on n_f such that, in the limit of high n_f, P_F will remain constant. This trend is apparent in Fig. 9 as the approach of P_F toward saturation at high values of n_f. As the precise dependences of the effective attenuation coefficients k_F and k_L on n_f are not known, their behavior is approximated by observing the dependence of α on n_f. As described in Sec. IV.A, the beam attenuation coefficient data for the 610-nm region were obtained from *in situ* transmissometry measurements. These data, which are presented in Fig. 10 as a function of n_f, demonstrate a strong linear relationship between α and n_f. As n_f approaches zero, α has a limiting and presumably constant background value of about 1.4 m^{-1} due to nonchlorophyllous particulate and dissolved materials and to water itself. At high values of n_f (~45 μg/l), the component of α due to the chlorophyll bearing phytoplankton is therefore about double the size of the background component. Assuming that both k_F and k_L exhibit a similar dependence on n_f, then both the numerator and denominator in Eq. (5) will tend to vary as n_f when attenuation becomes dominated by the chlorophyll a component; as a result, P_F will ultimately reach a saturated or constant value at high values of n_f.

The Raman-corrected fluorescence data P_F/P_R in Fig. 9 exhibits a considerable improvement toward linearity over that for P_F. The residual nonlinearity in the curve for P_F/P_R can be attributed to two possible sources.

First, with reference to that part of the flight line where the profiles of P_F and P_F/P_R are changing rapidly, i.e., between buoys 11′ and 13, it is possible that the lack of coincidence between n_f and P_F/P_R is due to a deviation in the laser fluorosensor flight line from the line defined by the ground truth sampling sites. The profile of P_F/P_R shown in Fig. 8 is also shown in Fig. 11 as the continuous line together with a profile of P_F/P_R obtained over the same nominal flight line ~20 min earlier and shown as the broken line. Although the reproducibility of the data is, in general, excellent, small differences between these two profiles are apparent in the region of buoys 12 and 13, presumably due to small differences between the two flight paths over the line of buoys. It is significant that the displacement of the earlier profile (broken line) from the later profile (continuous line) is in the direction tending to improve agreement between the airborne and ground truth data (see Fig. 8). However, as the precise direction of the

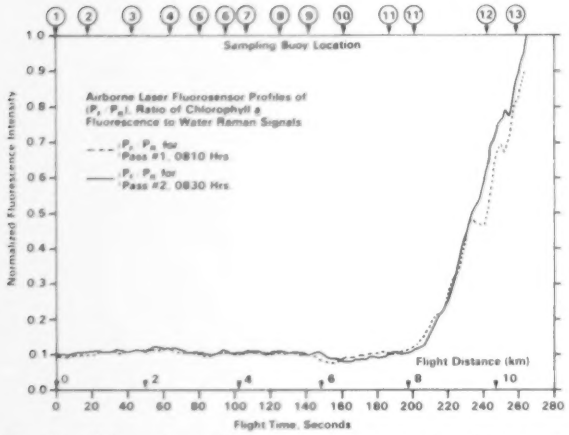

Fig. 11. Airborne laser fluorosensor profiles of P_F/P_R obtained 20 min apart over same region of Las Vegas Bay on 7 June 1979. Profiles smoothed using a moving 5-point average scheme.

gradient in n_f in relation to the flight line is not known, further speculation on this explanation for the residual nonlinearity in the plot of P_F/P_R vs n_f in Fig. 9 is not practical.

The second and possibly more plausible explanation for the residual nonlinearity in the plot of P_F/P_R vs n_f can be obtained by examining the suggestion that the ratio $(k_L + k_R)/(k_L + k_F)$ in Eq. (8) is not a constant as was assumed, but exhibits a weak direct dependence on n_f. This appears to be reasonable because numerous published attenuation spectra for both the beam and diffuse attenuation coefficients, respectively α and K, indicate that, as the concentration of the material in the water column responsible for attenuation increases, the changes in α and K are large in the blue and green regions, whereas changes in the red region near 685 nm, where attenuation is dominated by water itself, are generally relatively small.[15,29,39,40] Consequently, as n_f increases, $(k_L + k_R)/(k_L + k_F)$ will also increase although somewhat more slowly. In the limit of high n_f, this increase in $(k_L + k_R)/(k_L + k_F)$ will ultimately lead to saturation of P_F/P_R in a manner similar to that for P_F as described earlier. However, it has already been noted in Sec. II that variations in $(k_L + k_R)/(k_L + k_F)$ can be eliminated by tuning the water Raman band into coincidence with the chlorophyll a band at 685 nm, with the result that $k_F = k_R$ and $(k_L + k_R)/(k_L + k_F) = 1$. Unfortunately, as also noted in Sec. II, separation of these two overlapping quasi-Gaussian bands, which have similar bandwidths (~20 nm), would not be practical. A reasonable compromise might be achieved by employing laser excitation at 500 nm rather than at 470 nm, thereby shifting the water band from 560 to 603 nm. At this latter Raman wavelength, it is anticipated that the dependence of $(k_L + k_R)/(k_L + k_F)$ on the concentration of either chlorophyllous (phytoplankton) or nonchlorophyllous (suspended sediments and dissolved organics) materials will remain weak for all but the largest changes in optical attenuation.

Although not of immediate concern to the present discussion, it is noteworthy that extrapolations of the data for both P_F and P_F/P_R vs n_f in Fig. 9 do not pass through the origin as one would expect but rather intersect the abscissa at finite values of n_f (~3 μg/l). Three possible explanations for this anomaly are suggested.

First, the possibility that P_F may have been offset during either the detection, digitization, or recording stages or alternatively have been truncated during numerical analysis was not borne out by subsequent investigation.

Second, the possibility that a small but finite fraction of the extracted chlorophyllous material was nonfluorescent was examined. Figure 12 shows n_f for the 28 sampling sites plotted against the corresponding values for the *in situ* chlorophyll a fluorescence measurements made at 685 nm. These *in situ* fluorescence data were obtained using the flow-through field fluorometer with excitation at 440 nm as described in Sec. IV.A. As the extrapolation of these linearly distributed data points passes close to the origin, the suggestion that a fraction of the extracted chlorophyll a material is nonfluorescent does not appear to be realistic.

The third and most acceptable explanation is that the overall effective *in vivo* chlorophyll a excitation cross section for fluorescence emission at 685 nm when excited at 470 nm, denoted by σ_f in Eq. (1), is not constant as was assumed, but varies along the flight line because of changes in the relative concentrations of the different algal color groups in the surface water samples. Although a phytoplankton enumeration was not performed on the samples on the occasion of this flight, an enumeration performed on a set of samples obtained 10 days earlier indicated that significant changes occurred in the relative concentrations of the four dominant algal

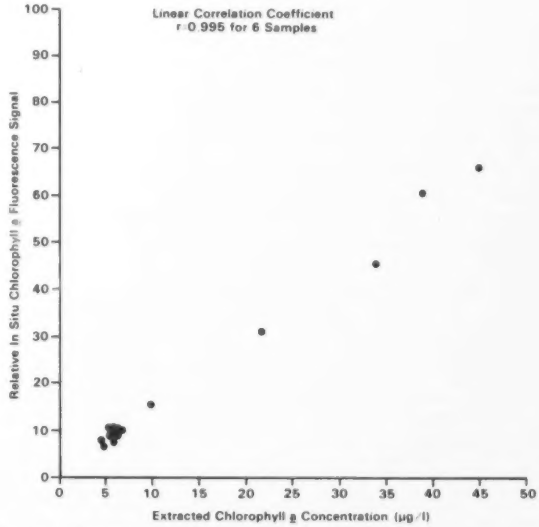
Linear Correlation Coefficient
r: 0.995 for 6 Samples
Relative In Situ Chlorophyll a Fluorescence Signal
Extracted Chlorophyll a Concentration (μg/l)

Fig. 12. Dependence of *in situ* chlorophyll a fluorescence measured with a field fluorometer using 440-nm excitation on chlorophyll a concentration n_f for the 28 sampling sites in Las Vegas Bay on 7 June 1979. Correlation coefficient is based on 6 samples, one of which is the mean of the group of 23 samples near the origin.

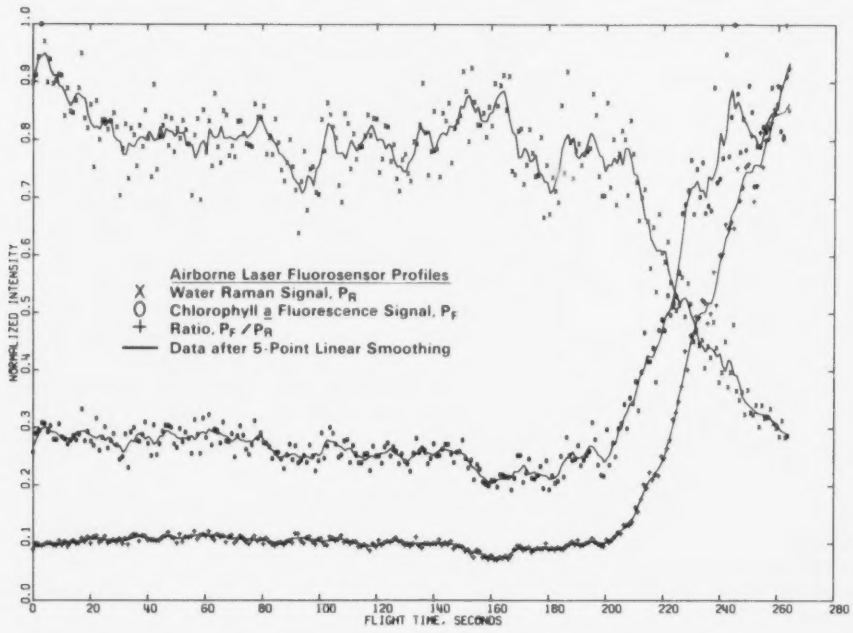
Airborne Laser Fluorosensor Profiles
X Water Raman Signal, P_R
O Chlorophyll a Fluorescence Signal, P_F
+ Ratio, P_F / P_R
Data after 5-Point Linear Smoothing
NORMALIZED INTENSITY
FLIGHT TIME, SECONDS

Fig. 13. Airborne laser fluorosensor profiles of P_F, P_R, and P_F/P_R for flight of 7 June 1979 over Las Vegas Bay before and after smoothing with a moving 5-point average scheme. Unsmoothed data are shown as discrete points and smoothed data as continuous lines.

color groups between buoys 1 and 13. Grab samples were found to contain primarily diatoms (bacillariophyta), dinoflagellates (pyrrophyta), green algae (chlorophyta), and yellow green algae (chrysophyta). As the flight line progresses from buoys 1 to 13, the diatoms exhibited a marked increase, the greens a relatively small increase, the yellow greens a relatively small decrease, and the dinoflagellates a marked decrease, with the largest changes occurring in the region between buoys 11 and 11′. It is in this region that the chlorophyll *a* ground truth data for the laser fluorosensor experiment begins to increase rapidly as one moves toward buoy 13 (see Fig. 8). However, the values of σ_f at 470 nm for three of the aforementioned algal color groups are known to be lower than the corresponding values at 440 nm[18] with the differences varying from group to group depending on the influence of different accessory pigments, such as the carotenes, xanthophylls, and chlorophyll *b*. In particular, dinoflagellates, which have a slightly lower excitation cross section at 470 nm than at 440 nm[18] were observed to be present between buoys 1 and 10 in concentrations ~10 times higher than those between buoys 10 and 13. Consequently, as the effective value for σ_f at 440 nm appears to have remained constant on the occasion of the laser fluorosensor flight as indicated by the linearly distributed data in Fig. 12, it is concluded that the failure of the data in Fig. 9 to extrapolate through the origin is due to a change in the effective value of σ_f at 470 nm along the flight line, mainly involving the clusters of data in Fig. 9 representing P_F and P_F/P_R for the 23 sampling sites between buoys 1 and 11.

As described in Sec. IV.B, the data used to form the laser fluorosensor profiles for P_F, P_R, and P_F/P_R in Fig. 8 were smoothed using a moving 5-point average scheme. In addition to reducing the amplitude of system noise and small scale (high-frequency) fluctuations caused by horizontal patchiness in the phytoplankton population density, this particular smoothing procedure also produces a 5-times reduction in the effective ground resolution element size of the airborne profiles from 30 to 150 m. The effects of this smoothing procedure on the profiles of P_F, P_R, and P_f/P_R are demonstrated in Fig. 13. The unsmoothed data are represented by the discrete values for each record, and the corresponding smoothed data by the continuous profiles. Large excursions exist in the unsmoothed data for P_F because of the dependence of P_F both on small scale horizontal variations in n_f and on similar variations in k_F and k_L produced by the same variations in n_f.

Examination of these profiles shows that the Raman correction procedure effects a significant reduction in the small scale fluctuations in the unsmoothed data for P_F/P_R when compared with those for the corresponding unsmoothed data for P_F. This reduction occurs because the small scale variability in P_F produced by changes in k_L and k_F is closely matched by a similar variability in P_R produced by changes in k_L and k_R; the amplitude of the peak-to-peak signal fluctuations over a 20-sec interval in the unsmoothed data for P_F/P_R are approximately 40% less than those of the corresponding unsmoothed data for P_F. As a result of the reduction in amplitude of these small scale fluctuations, requirements for smoothing the profiles could be relaxed to (say) a 3-point averaging procedure or, alternatively, eliminated altogether, thereby preserving real information relating to small scale horizontal variations in the substance being monitored, viz. the chlorophyll *a* concentration.

On the basis of the observed results, it is concluded

that the Raman normalization procedure is a highly effective method for correcting the chlorophyll *a* fluorescence data for changes in optical attenuation between sample locations produced by changes in concentration of the chlorophyllous materials (phytoplankton), whether these be small changes over short distances or large changes over long distances.

B. Raman Correction of Attenuation by Suspended Sediments

So far, the changes that have been observed in P_F due to variations in k_L and k_F have been caused by variations in the phytoplankton population density, as represented by the chlorophyll *a* concentration n_f. This is characterized in the profiles shown in Fig. 8 by the steady fall in the water Raman signal P_R along the flight line in conjunction with the concurrent rise in the chlorophyll *a* fluorescence signal P_F. In addition, it has been shown that, when optical attenuation in the water column is due predominantly to the presence of phytoplankton, the chlorophyll *a* fluorescence signal P_F measured by the laser fluorosensor tends towards saturation. In simple terms, as the phytoplankton population density, represented by n_f in Eq. (5), increases, optical attenuation, as represented by k_L and k_F in Eq. (5), also increases, producing a corresponding reduction in P_F. However, in the limit when attenuation in the water column is due solely to the phytoplankton, this reduction in P_F is exactly compensated by a corresponding increase caused by increasing n_f. In the absence of Raman correction, P_F then remains constant regardless of changes in n_f.

The other case in which changes in optical attenuation are due to changes in the concentrations of nonchlorophyllous materials such as suspended sediments and dissolved organics is characterized by situations in which changes in P_F are directly related to changes in P_R, i.e., a decrease in P_R is accompanied by a corresponding decrease in P_F. This is in direct contrast to the previous case in which attenuation, due predominantly to chlorophyllous materials in the water column, causes P_F to exhibit an inverse relationship with P_R, leading ultimately to saturation of P_F at high n_f.

Examples of both situations can be seen in the laser fluorosensor profiles shown in Fig. 14 and obtained on 23 May 1979 over the same flight line. The steady increase in P_F as the flight line progresses from buoy 1 to buoy 13, which is due to a corresponding increase in n_f, is accompanied by a steady and predictable decline in P_R produced by this same increase in n_f. The other phenomena apparent in Fig. 14 are the relatively large and sudden changes that can be seen in the profiles of P_F and P_R, particularly between buoys 1 and 7. The direct relationship between the changes in P_F and those in P_R, which is confirmed by the absence of these artifacts in the profile for P_F/P_R, suggests that they are caused by changes in optical attenuation in the water column due to the presence of nonchlorophyllous material. The influence of changes in surface reflectivity on the laser beam and on the backscattered fluorescence and Raman signals is not considered to be a contributing factor for operations close to normal incidence, provided that breaking water is not present.[41]

Examination of the video recordings for this flight line indicated that these anomalies in the profiles of P_F and P_R, involving higher than normal values for these parameters and located in the regions of buoys 2, 4, and 6, corresponded to narrow, well-defined channels of relatively dark, clear water. In particular, the anomaly close to buoy 6 was found to correspond to the residual wake of the launch being used to collect the ground truth grab samples. On subsequent flights over this region of Lake Mead during periods of low wind speed and relatively high temperatures, the water surface was seen to be covered by a random network of intersecting, dark channel-like bands presumably made by pleasure craft. An absence of boat traffic in the immediate vicinity of most of these bands suggests that, in the absence of wind-induced mixing, the bands are dimensionally stable and may have been produced several hours prior to being sighted.

Although not confirmed by independent investigation, the presumably higher turbidity of the waters adjacent to these bands of relatively clear water is believed to be a manifestation of calcite ($CaCO_3$) precipitation, a condition often referred to as "whiting" or milky water phenomenon.[42] The mechanisms involved in carbonate saturation and precipitation are not well understood, but important contributing factors are higher than normal temperatures in the epilimnion that lowers the solubility of $CaCO_3$, an increase in pH due to high phytoplankton productivity that results in higher CO_3^{2-} activities, high alkalinity, and a high Ca^{2+} ion concentration.[42] It is significant that all these conditions are typical of the surface layers of the Las Vegas Bay region of Lake Mead during spring bloom in late May and early June. Strong and Eadie,[42] who made an extensive investigation of the extent of this

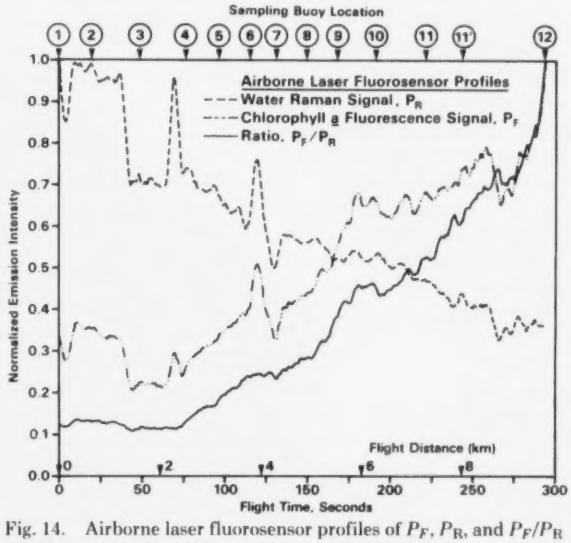

Fig. 14. Airborne laser fluorosensor profiles of P_F, P_R, and P_F/P_R for flight of 23 May 1979 over Las Vegas Bay. Profiles smoothed using a moving 5-point average scheme.

phenomenon in the Great Lakes over a period of several years using LANDSAT multispectral imagery, indicated that the concentration of this carbonate precipitate is a maximum several meters below the surface.

Assuming that calcite precipitation is the cause of the optical artifacts observed on the occasion of the overflight of 23 May 1979 and that the precipitate existed as a well-defined layer within the first optical attenuation length, one can then expect the passage of a boat to disperse this layer of suspended particulate material both to deeper and shallower depths. The net effect of this local disturbance is therefore a lowering of the effective attenuation coefficients k_L, k_R, and k_F in relation to the adjacent waters resulting in an apparent increase in clarity of the surface waters and in an increase in both P_F and P_R as indicated by the profiles in Fig. 14. This phenomenon was not observed in the profiles for the flight of 7 June 1979 shown in Fig. 8, presumably because of the dispersive effects of the relatively strong wind encountered on this occasion; evidence for the effect of the strong wind-induced surface mixing is manifested in Fig. 8 by a general absence of small scale, large amplitude fluctuations in the profile for P_F/P_R.

The ability of the Raman correction method to rectify the chlorophyll *a* fluorescence data for the effects of attenuation produced by this suspended sediment layer is a little surprising as the validity of the laser fluorosensor equation [Eq. (1)] is based on the assumption that all materials, both fluorescent and nonfluorescent, are uniformly distributed in the water column. However, on the basis of this observation, it is probably safe to conclude that the Raman correction method is highly effective in being able to correct the chlorophyll *a* fluorescence data for the effects of attenuation produced by changes in concentration of nonchlorophyllous materials between sample locations, whether these be suspended sediments or dissolved organics.

C. Remote Measurement of Optical Attenuation using Water Raman Emisssion

Inspection of Eq. (3) suggests that P_R can be used to make relative measurements of the term $(k_R + k_L)$. As n_w, σ_w, and d_r are all deemed to be constant and as values of P_L and H are recorded concurrently with P_R, then the term $(P_R H^2/P_L)$ can be expected to vary as $(k_R + k_L)$. Defining k_v as the mean of k_R and k_L and, as such, to be the effective attenuation coefficient representative of some visible wavelength v intermediate between the Raman and laser wavelengths, one can simplify Eq. (3) to the form

$$k_v = C_3 P_R^{-1}, \tag{10}$$

where P_R has been normalized for variations in P_L and H, and C_3 is a proportionality constant analogous to the constants in Eqs. (2) and (9).

Due to its dependence on the laser fluorosensor system constants in Eq. (4), C_3 should be determined on the occasion of each mission by making ground truth measurements of k_v at a small number of selected reference sites under the aircraft flight path concurrent

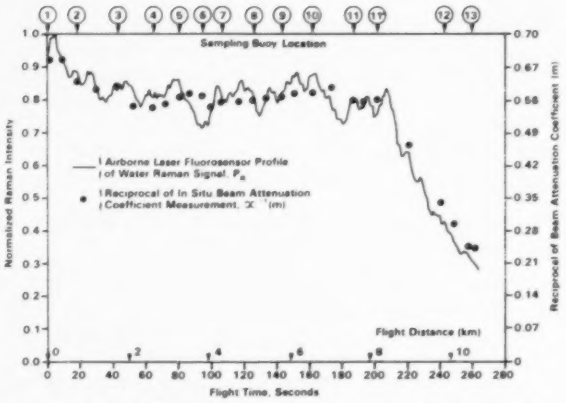
Sampling Buoy Location
Airborne Laser Fluorosensor Profile of Water Raman Signal, P_R
Reciprocal of In Situ Beam Attenuation Coefficient Measurement, α^{-1} (m)
Normalized Raman Intensity
Reciprocal of Beam Attenuation Coefficient (m)
Flight Distance (km)
Flight Time, Seconds

Fig. 15. Airborne laser fluorosensor profile of water Raman emission signal P_R for flight of 7 June 1979 overlayed with normalized values for the reciprocal of the beam attenuation coefficient α^{-1} obtained from *in situ* measurements at the 28 sampling sites in Las Vegas Bay at the time of the overflight.

with the airborne measurements of P_R^{-1}. Unfortunately, as discussed in Sec. II, k_v is dependent on artifacts introduced by the monitoring system in addition to the nature of the water sample and, as a result, *in situ* methods for its measurement do not exist. It is therefore proposed that one or the other of the two established water quality parameters K_v and α_v, respectively the diffuse and beam attenuation coefficients at wavelength v, be substituted for k_v in Eq. (10). This can be justified on two grounds; first, k_v relevant to the laser fluorosensor application has values lying intermediate between those for K_v and α_v (see Sec. II), and second, K_v and α_v are known to be closely related through the existence of empirical relationships of the form[20,21] $K = 0.2\,\alpha + 0.04$. For the purpose of the present experiments, α_v is the preferred standard against which P_R^{-1} is to be compared, first, because it can be readily measured on a continuous basis and, second, because it is a property of the water sample alone, independent of the incident radiance distribution.

The existence of a close linear relationship between P_R^{-1} and α is confirmed by the data presented in Fig. 15. Here, the profile of P_R for the laser fluorosensor flight of 7 June 1979 is overlayed with least squares normalized values of α^{-1} (measured at 610 nm) that were obtained for the 28 sampling sites at the time of the overflight. These same data for α are shown in Fig. 16 plotted against the corresponding values of P_R^{-1} obtained over the 28 sampling sites. This plot indicates a high degree of correlation between α and P_R^{-1} and appears, on extrapolation, to pass close to the origin. It should be noted that this correlation exists in spite of both the possible differences between k and α and the fact that α was measured at 610 nm rather than at a wavelength characteristic of k_v between 470 and 520 nm.

It is therefore suggested that this linear relationship between P_R^{-1} and α be exploited as a method for remote sensing the beam attenuation coefficient to be used in preparing maps showing isopleths of α for the surface layer defined by the attenuation length α^{-1}.

VI. Conclusions

This study is an investigation of the merits of using the concurrent water Raman emission as a means for correcting the fluorescence emitted from a uniformly distributed surface water fluorophore for variations induced by changes in optical attenuation. Conclusions and observations concerning this method and recommendations concerning its future implementation are summarized as follows:

(1) Raman correction of the fluorescence emission is seen to be highly effective in eliminating artifacts from the fluorescence data introduced by both small (horizontal) scale, low amplitude and large (horizontal) scale, high amplitude changes in optical attenuation. In the present study involving the measurement of chlorophyll *a* fluorescence, these variations in attenuation were due to changes in concentration of both chlorophyllous and nonchlorophyllous particulate materials. However, the authors see no reason why this technique will not be equally effective in correcting for changes in attenuation produced by point-to-point variations in concentration of dissolved materials that are uniformly distributed in the water column, such as dissolved organics, whether these materials be fluorescent or nonfluorescent. The technique is successful because the concurrent Raman emission emanates from essentially the same sample volume as does the fluorescence emission and therefore undergoes the same attenuation processes provided that the fluorescence and Raman emission wavelengths are not widely separated. A residual nonlinearity in the Raman corrected fluorescence data of the present experiments is probably due to the attenuation of the water Raman emission at 560 nm being, to some extent, nonrepresentative of attenuation of the chlorophyll *a* fluorescence emission at 685 nm. It is suggested that laser excitation at 500 nm producing water Raman emission at 603 nm be preferred to excitation 470 nm as used here. This compromise will minimize the wavelength separation while avoiding overlap of the water Raman and chlorophyll *a* fluorescence emission bands.

(2) Raman correction of the fluorescence data eliminates problems due to both short-term (within mission) and long-term changes in system sensitivity that have an equal influence on both the fluorescence and Raman signals. Such changes include but are not restricted to both pulse-to-pulse fluctuations and long-term drift in laser output power, line voltage changes, and amplifier gain drift.

(3) As both the fluorescence and Raman signals exhibit a $1/H^2$ dependence on changes in target range H, the fluorescence to Raman signal ratio P_F/P_R is independent of these changes.

(4) As the effect of changes in water surface reflectivity due either to wave action or to off-nadir operation of the laser fluorosensor are essentially the same for both the fluorescence and Raman signals, the fluorescence to Raman signal ratio P_F/P_R is independent of these changes.

(5) Use of the concurrent water Raman return to correct for variations in laser beam penetration is ideal because its implementation requires no information, either theoretical or experimental, to describe the effective attenuation coefficient relevant to the laser fluorosensor application.

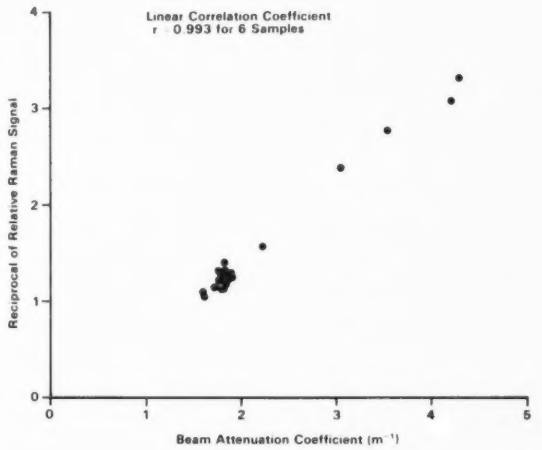

Fig. 16. Variation of P_R^{-1} with beam attenuation coefficient α for the 28 sampling sites in Las Vegas Bay on 7 June 1979. Airborne data taken from the smoothed laser fluorosensor profile for P_R. Correlation coefficient is based on 6 samples, one of which is the mean of the group of 23 samples near the origin.

(6) Laser fluorosensor measurements of chlorophyll *a* concentration and beam attenuation coefficient are relative and therefore need to be calibrated either by obtaining grab samples (for laboratory analysis) or by making *in situ* ground truth measurements at a small number of reference sites under the sensor flight path at the time of the airborne mission.

(7) The water Raman emission signal used in this study to correct the chlorophyll *a* fluorescence signal and for making relative measurements of the beam attenuation coefficient was actually the combined intensity of the water Raman emission and a nontrivial background emission due to the fluorescence of dissolved organics. Provided that the intensity of this background fluorescence remains constant and the materials producing it are uniformly distributed in the water column, this expedient is acceptable. However, for most fresh waters, this organics-related background fluorescence emission is rarely constant or negligible across the extent of a water body and must be subtracted from the Raman signal by use of two additional fluorescence measurements made on either side of the Raman band.

(8) The reciprocal of the water Raman emission signal P_R^{-1} has been shown to vary directly as the beam attenuation coefficient α. This is in general agreement with the theoretical prediction that P_R^{-1} varies as k_v, the effective attenuation coefficient at some wavelength v intermediate between those for the laser and Raman emission. It is suggested that this relationship be exploited as a method for remote sensing the beam attenuation coefficient of surface waters.

References

1. J. F. Fantasia and H.C. Ingrao, "Development of an Experimental Airborne Laser Remote Sensing System for the Detection and Classification of Oil Spills," in *Proceedings, Ninth International Symposium on Remote Sensing of the Environment, 15–19 Apr. 1974* (Environmental Research Institute of Michigan, Ann Arbor, 1974), p. 1711.
2. R. A. O'Neil, L. Buja-Bijunas, and D. M. Rayner, Appl. Opt. **19,** 863 (1980).
3. F. E. Hoge and R. N. Swift, Appl. Opt. **19,** 3269 (1980).
4. P. B. Mumola, O. Jarrett, and C. A. Brown, "Multiwavelength Laser Induced Fluorescence of Algae *in-vivo:* A New Remote Sensing Technique," in *Proceedings, Second Joint Conference on Sensing of Environmenal Pollutants, Washington, D.C., 10–12 Dec. 1973,* p. 53.
5. M. Bristow, D. Nielsen, and R. Furtek, "A Laser-Fluorosensor Technique for Water Quality Assessment," in Proceedings, *Thirteenth International Symposium on Remote Sensing of the Environment, 23–27 Apr. 1979* (Environmental Research Institute of Michigan, Ann Arbor, 1979), p. 397.
6. F. H. Farmer, C. A. Brown, O. Jarrett, J. W. Campbell, and W. Staton, "Remote Sensing of Phytoplankton Density and Diversity in Narragansett Bay using an Airborne Fluorosensor," in *Proceedings, Thirteenth International Symposium on Remote Sensing of the Environment, 23–27 Apr. 1979* (Environmental Research Institute of Michigan, Ann Arbor, 1979), p. 1793.
7. J. F. Fantasia, T. M. Hard, and H.C. Ingrao, "An Investigation of Oil Fluorescence as a Technique for Remote Sensing of Oil Spills," Final Report, DOT-TSC-USCG-71-7, NTIS PB204-792 (June 1971).
8. R. Horvath, W. L. Morgan, and S. R. Stewart, "Optical Remote Sensing of Oil Slicks: Signature Analysis and Systems Evaluation," Final Report, Contract DOT-USCG 92580-A, Project 724104.2/1, Willow Run Laboratories, U. Michigan, Ann Arbor (Oct. 1971).
9. R. M. Measures and M. P. F. Bristow, "The Development of a Laser Fluorosensor for Remote Environmental Probing," AIAA Paper 71-1121, in *Proceedings, Joint Conference on Sensing of Environmental Pollutants, Palo Alto, California, 8–10 Nov. 1971* (American Institute of Aeronautics and Astronautics, New York 10017, 1971).
10. E. J. Friedman and G. D. Hickman, "Laser Induced Fluorescence in Algae: A New Technique for Remote Detection," Final Report, sponsored by NASA, Wallops Island under Contract NAS 6-02081, Sparcom, Inc., Alexandria, Virginia (Oct. 1971).
11. E. V. Browell, "Analysis of Laser Fluorosensor Systems for Remote Algae Detection and Quantification," NASA Technical Note TN D-8447, NASA, Washington, D.C. (June 1977).
12. R. E. Morrison, J. Geophys. Res. **75,** 612 (1970).
13. D. A. Kiefer and R. W. Austin, Limnol. Oceanogr. **19,** 55 (1974).
14. J. G. Shannon, "Light Attenuation Measurements with a Unique Transmissometer System," IEEE International Conference on Engineering in the Ocean Environment, Halifax, 21–23 Aug. 1974, IEEE Publication 74CH0 873-0 OCC (1974).
15. N. G. Jerlov, *Marine Optics* (Elsevier,Amsterdam, 1976), p. 47.
16. A. J. Campillo, V. H. Kollman, and S. L. Shapiro, Science **193,** 227 (1976).
17. C. A. Brown, F. H. Farmer, O. Jarrett, and W. L. Staton, "Laboratory Studies of *In Vivo* Fluorescence of Phytoplankton," in *Proceedings, Fourth Joint Conference on Sensing of Environmental Pollutants, New Orleans, Louisiana, 6–11 Nov. 1977* (American Chemical Society, Washington, D.C., 1978), p. 782.
18. C. S. Yentsch and C. M. Yentsch, J. Mar. Res. **37,** 471 (1979).
19. H. H. Kim, Appl. Opt. **16,** 46 (1977).
20. J. G. Shannon, "Correlation of Beam and Diffuse Attenuation Coefficients Measured in Selected Ocean Waters" in *Proceedings, SPIE Conference on Ocean Optics, 19–20 Aug. 1975* (SPIE, New York, 1975), Vol. 64, p. 3.
21. G. S. Ofelt, "Relation Between Beam and Diffuse Attenuation Coefficients in the Lower Chesapeake Bay Area," Institute of Oceanography, Old Dominion University, Norfolk, Va., Technical Report 32 (Oct. 1976).
22. M. P. F. Bristow, D. Nielsen, D. Bundy, R. Furtek, and J. Baker, "Airborne Laser Fluorosensing of Surface Water Chlorophyll *a*," U.S. Environmental Protection Agency, Las Vegas, NV, Project Report EPA-600/4-79-048 (Aug. 1979).
23. M. P. F. Bristow, W. R. Houston, and R. M. Measures, "Development of a Laser Fluorosensor for Airborne Surveying of the Aquatic Environment," in *Proceedings of the Symposium on the Use of Lasers for Hydrographic Studies, NASA Wallops Island, Va., 12 Sept. 1973* (NASA Special Publication SP 375, Washington, D.C., 1975).
24. M. P. F. Bristow and D. Nielsen, "Remote Monitoring of Organic Carbon in Surface Waters," U.S. Environmental Protection Agency, Las Vegas, Nev., Project Report EPA-600/4-81-001 (Feb. 1981).
25. G. E. Walrafen, J. Chem. Phys. **47,** 114 (1967).
26. C. H. Chang and L. A.Young, "Seawater Temperature Measurement from Raman Spectra," AVCO Research Note 960, AVCO Everett Research Laboratory Inc., Everett, Mass. (Jan. 1974).
27. P. L. Smart, B. L. Finlayson, W. D. Rylands, and C. M. Ball, Water Res. **10,** 805 (1976).
28. 7-dimethylamino-4-methyl coumarin, Eastman Organic Chemicals, Rochester, N.Y.
29. R. C. Smith and J. E. Tyler in *Photochemical and Photobiological Reviews* (Plenum, New York, 1976), Vol. 1, p. 117.
30. M. P. F. Bristow, Appl. Opt. **18,** 952 (1979).
31. D. A. Kiefer, Mar. Biol. **23,** 39 (1973).
32. D. A. Kiefer, Mar. Biol. **23,** 263 (1973).
33. D. Blasco, "Variations of the Ratio *in vivo*—Fluorescence/*a*—Chlorophyll and its Applications to Oceanography. Effect of Limiting Different Nutrients, of Night and Day and Dependence on the Species Under Investigation," NASA Technical Translation TTF—16,317, 1975 from original in Spanish, published in Investigacion Pesquera **37,** 533 (1973).
34. M. E. Loftus and H. H. Seliger, Chesapeake Sci. **16,** 79 (1975).
35. S. I. Heaney, Freshwater Biol. **8,** 115 (1978).
36. J. D. H. Strickland and T. R. Parsons, *A Practical Handbook of Seawater Analysis* (Fisheries Research Board of Canada, Ottawa 1972), Part 4, Section 3.1, Spectrophotometric Determination of Chlorophylls and Total Carotenoids.
37. R. Furtek, "Extraction and Analysis of Chlorophyll *a* and Associated Problems," U.S. Environmental Protection Agency, Las Vegas, Project Summary (1981).
38. M. F. Baudouin and P. Scoppa, Mar. Biol. **10,** 66 (1971).
39. E. O. Hulburt, J. Opt. Soc. Am. **35,** 698 (1945).
40. R. C. Smith and K. S. Baker, Photochem. Photobiol. **29,** 311 (1979).
41. D. M. Rayner, M. Lee, and A. G. Szabo, Appl. Opt. **17,** 2730 (1978).
42. A. E. Strong and B. J. Eadie, Limnol. Oceanogr. **23,** 877 (1978).